

An Elastic Autonomous Self-Healing Capacitive Sensor Based on a Dynamic Dual Crosslinked Chemical System

Qihong Zhang, Simiao Niu, Li Wang, Jeffrey Lopez, Shucheng Chen, Yifeng Cai, Ruichun Du, Yuxin Liu, Jian-Cheng Lai, Ling Liu, Cheng-Hui Li, Xuzhou Yan, Chungeng Liu, Jeffrey B.-H. Tok, Xudong Jia,* and Zhenan Bao*

Adopting self-healing, robust, and stretchable materials is a promising method to enable next-generation wearable electronic devices, touch screens, and soft robotics. Both elasticity and self-healing are important qualities for substrate materials as they comprise the majority of device components. However, most autonomous self-healing materials reported to date have poor elastic properties, i.e., they possess only modest mechanical strength and recoverability. Here, a substrate material designed is reported based on a combination of dynamic metal-coordinated bonds (β -diketone–europium interaction) and hydrogen bonds together in a multiphase separated network. Importantly, this material is able to undergo self-healing and exhibits excellent elasticity. The polymer network forms a microphase-separated structure and exhibits a high stress at break (≈ 1.8 MPa) and high fracture strain ($\approx 900\%$). Additionally, it is observed that the substrate can achieve up to 98% self-healing efficiency after 48 h at 25 °C, without the need of any external stimuli. A stretchable and self-healable dielectric layer is fabricated with a dual-dynamic bonding polymer system and self-healable conductive layers are created using polymer as a matrix for a silver composite. These materials are employed to prepare capacitive sensors to demonstrate a stretchable and self-healable touch pad.

Stretchable electronics have attracted significant attention recently for their applications in e-wear and e-skin.^[1] Different approaches, such as organic electronics,^[2] thin film electronics,^[3] and flexible inorganic electronics,^[4] have

been developed to realize the wearable electronics. Due to our daily active body movements, these electronics (especially when located at the joints) are susceptible to either ruptures or scratches. Therefore, to extend the device operational lifetime, it is imperative to provide a protective barrier against environmental stimuli, while maintaining the electronics' robust mechanical properties. Self-healing is essential for wearable systems, and incorporating some forms of autonomous and repeatable self-healing into electronic devices would enhance their robustness and durability. Several strategies based on the bond reformation, such as the employment of reversible covalent bonds,^[5] and the introduction of dynamic noncovalent bonds,^[6] have been reported to enable self-healing polymers. However, the majority of these self-healing polymers either require external stimuli, e.g., light,^[6,7] heat,^[8] solvent,^[9] and pressure,^[10] or suffer from poor elasticity.^[6e] It is important to note that achieving both elasticity and self-healing properties simultaneously is difficult, because most elastomers, such as polyisoprene or poly(dimethylsiloxane) (PDMS), depend on strong covalently bonded crosslinks.^[11] In traditional elastomers, the entropy of hindered or aligned


Dr. Q. Zhang, L. Wang, Y. Cai, R. Du, Prof. X. Jia
Key Laboratory of High Performance Polymer Material
and Technology of MOE
Department of Polymer Science and Engineering
School of Chemistry and Chemical Engineering
Nanjing University
Nanjing 210093, P. R. China
E-mail: jiaxd@nju.edu.cn

Dr. Q. Zhang, Dr. S. Niu, Dr. J. Lopez, S. Chen, Dr. X. Yan,
Dr. J. B.-H. Tok, Prof. Z. Bao
Department of Chemical Engineering
Stanford University
Stanford, CA 94305, USA
E-mail: zbao@stanford.edu

Y. Liu
Department of Bioengineering
Stanford University
Stanford, CA 94305, USA

J.-C. Lai, Dr. C.-H. Li, Prof. X. Jia
State Key Laboratory of Coordination Chemistry
Collaborative Innovation Center of Advanced Microstructures
Nanjing University
Nanjing 210093, P. R. China

L. Liu, Prof. C. Liu
Institute of Theoretical and Computational Chemistry
Key Laboratory of Mesoscopic Chemistry of the Ministry of Education
(MOE)
Nanjing University
Nanjing 210093, P. R. China

 The ORCID identification number(s) for the author(s) of this article can be found under <https://doi.org/10.1002/adma.201801435>.

DOI: 10.1002/adma.201801435

polymer chain decreases at higher strain and allows the material to recover to its original state driven by entropic gain.^[12] On the other hand, most self-healing systems rely on the weak dynamic noncovalent interactions to recover the material's properties.^[6d,e] Polymer chains connected by weak dynamic bonds break more readily allowing energy dissipation at higher strain, which invariably leads to poor recovery behavior. Therefore, the challenge remains to create materials that have both good elastic performance and autonomous healing capability.

For weak crosslinks, they are easily broken upon loading. For example, the binding energy of hydrogen bonds is relatively weak^[13] (e.g., 15–18 kcal mol⁻¹ for amides^[14] and 14–22 kcal mol⁻¹ for urethanes^[15]) and would break readily under strain. To address this limitation, conferring strong yet dynamic crosslinks in polymer network has been implemented. Wu et al. reported a hybrid network by combining reversible hydrogen bond and covalent crosslinks to generate a tough elastomer with a 30% healing efficiency after 12 h at room temperature.^[16] Park and co-workers introduced aromatic disulfide as dynamic covalent bond into thermoplastic polyurethane and reached a self-healing elastomer with high tensile strength and toughness.^[17] Xu and co-workers reported a self-healing conductor based on dual-dynamic hydrogen bonding and electrostatic interactions, and further demonstrated sensitive strain and pressure sensor.^[18] Zhou and co-workers designed a self-healable sensor with positive/negative piezoresistivity based on the design of hierarchical structure connected through supramolecular metal–ligand (M–L) coordination bonds.^[19] Guan and co-workers reported a multiphase supramolecular strategy to prepare self-healable thermoplastic elastomers.^[20] M–L interactions are promising as dynamic healing motifs because the thermodynamic and kinetic parameters of M–L complexes are tunable over a broad range, which could potentially yield self-healing materials with highly adjustable mechanical properties.^[9,21] In addition, thermodynamic incompatibility induced microphase separation will promote the elastic performance of the materials.^[22] Hydrogen bonding plays an important role to generate microphase separation between different phases well known for the case of polyurethane and polyurea.^[23] Moreover, the system with relatively high M–L binding constants also tends to phase separate with the M–L complexes residing in hard glassy or crystalline domains, thus contributing to the reinforcement of mechanical properties.

We propose here a molecular design in using dual-dynamic crosslinking system, which possess a combination of hydrogen bonding and dynamic M–L coordination, to enable microphase separation in the bulk and, as such, facilitating the self-healing process and conferring good elastic property. The mechanical stress at break of the material reaches 1.8 MPa and the strain at break is observed at about 900% ($\lambda = 10$). The material could recover to 1.2× its original length after a process of stretching to 500% ($\lambda = 6$) and unloading the sample, and fully recovered to its original length with a 30 min relaxation. The damaged samples can achieve up to 98% healing efficiency after 48 h at room temperature without stimuli. We fabricated a capacitive touch sensor array using our prepared elastic and self-healable material as the dielectric substrate and the matrix for a conductive composite.

We reasoned that a higher coordination number of the metal center would result in higher crosslinking densities, which would then reduce the overall chain sliding when subjected to high strain. Herein, we chose Eu(III)–curcumin coordination complex for our design. Curcumin was natural occurring chelating agent, due to the β -diketone moiety. It had been successfully used to coordinate with different metal ions especially the lanthanide elements.^[24] To investigate the coordination structure in the polymer network, we chose the M–L curcumin-A (Figure S1a, Supporting Information) and Eu(CF₃SO₃)₃. The binding energy between Eu and curcumin is 38.5 kcal mol⁻¹ per Eu–O bond, as was calculated by a model coordination complex (see Supporting Information *binding energy of Eu–O* and Table S1, Supporting Information). The binding energy of the coordination bond is stronger than hydrogen bonding. We also observed that the coordination structure with a stoichiometry of 3:1 curcumin to Eu(CF₃SO₃)₃ showed a maximum peak at ≈ 450 nm, as confirmed by UV–vis spectrum (Figure 1c). This was attributed to the formation of the specific 3:1 curcumin:Eu complex. In addition, molecular weight of the coordinates tested by mass spectra indicated that the coordination number between Eu³⁺ and curcumin of the stable complexes was 1:3. (Figure S1c, d, Supporting Information).

To increase the miscibility between different phases and to promote self-healing, we chose urethane linkages as they have a much higher content of hydrogen bonding between the N–H and C=O groups. Furthermore, we introduced β -diketonate ligands to the polymer chain, as they were capable of crosslinking via both hydrogen bondings and dynamic M–L coordinations. We first prepared the curcumin polymer block (termed **P-Cur**; structure shown in Figure 1a) by step polymerization. Curcumin was initially reacted with excess IPDI at 90 °C to form a monomer featuring isocyanate terminated groups. Subsequent addition of polytetramethylene ether glycol ($M_n = 2000$) and chain extender 1,4-butanediol to the monomer afforded the desired **P-Cur** polymer (Figure S2a, Supporting Information). ¹H NMR showed multiple peaks around 7.0 ppm, indicating the curcumin was incorporated in the polymer chain (Figure S2b, Supporting Information). The structure of the P-Cur was characterized by fourier transform infrared spectroscopy (FT-IR), showing that all the NCO groups were fully reacted (Figure S3, Supporting Information). In addition, gel permeation chromatography (GPC) measured average molecular weights of the P-Cur were $M_w = 120$ kDa and $M_n = 37$ kDa. After coordination of Eu(III), the linear chains were further crosslinked by coordination bonds, resulting in the formation of a polymer network (termed as **P-Cur-Eu**). The appearance of C=O at 1625 cm⁻¹ was indicative of the presence of curcumin moiety. Upon the addition of Eu³⁺, the disappearance of the C=O vibration feature indicated the coordinations of Eu and curcumin O (Figure 1d and Figure S3, Supporting Information). Morphology of the coordinated crosslinked polymer as observed by transmission electron microscopy (TEM) showed that aggregation of ≈ 20 nm from Eu-complexation was uniformly distributed in the polymer matrix (Figure 1e), and the average distance between two phases was ≈ 40 nm, as confirmed by small-angle X-ray scattering (Figure S4, Supporting Information).

P-Cur was observed to be a soft tacky film without any appreciable mechanical properties, measured with ≈ 0.1 MPa tensile stress and 3000% elongation (Figure S5, Supporting

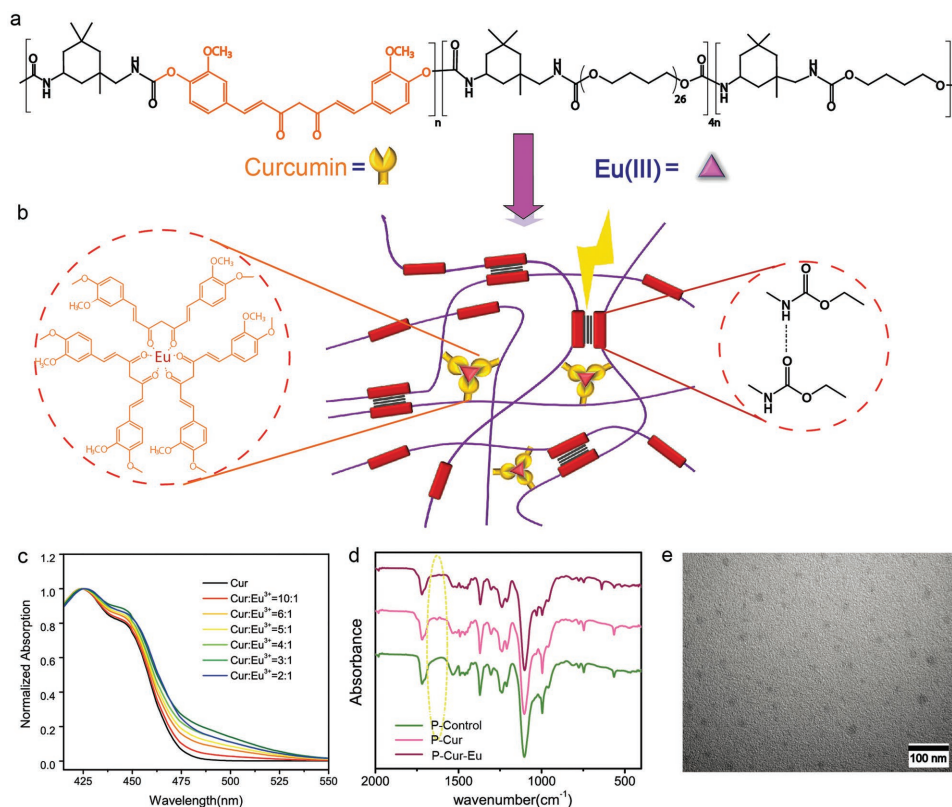


Figure 1. a) Molecular structure of curcumin (Cur)-embedded polymer. b) A schematic depiction of Eu (III) coordinated P-Cur material, highlighting the Eu–curcumin coordination bonds and the hydrogen bond derived from the urethane groups. c) UV–vis spectra of samples with different ratios of curcumin/Eu in THF. The curves were normalized using the absorption band at 425 nm. d) FT-IR of different samples. e) TEM image of dynamic interaction system in the **P-Cur-Eu = 3:1** substrate. Scale bar: 100 nm.

Information). To confer the material with more toughness and elastic property, we proceed to investigate if the addition of $\text{Eu}(\text{CF}_3\text{SO}_3)_3$ to **P-Cur** would enhance their mechanical performance.

We investigated the effect of the coordination between the metal ions and the ligand blocked polymer. Control samples which include: i) no curcumin (termed **P-Control**) and ii) mixed with the $\text{Eu}(\text{CF}_3\text{SO}_3)_3$ (**P-Control-Eu**) were both prepared (see the Supporting Information). Frequency-dependent dynamic moduli of **P-Control**, **P-Control-Eu**, **P-Cur**, and **P-Cur-Eu** were investigated by small-amplitude oscillatory shear. As shown in Figure S6 in the Supporting Information, introduction of Eu^{3+} into the **P-Control** (which lacks β -diketone ligands in the main chain) did not improve the mechanical property of polymer. On the other hand, addition of Eu^{3+} to **P-Cur** was observed to significantly enhance the mechanical strength of the polymer. Specifically, an increase in dynamic storage modulus of several orders of magnitude was observed. This experiment together with the disappearance of $\text{C}=\text{O}$ vibration in FT-IR clearly indicated that there were coordination interactions between the curcumin ligand and Eu^{3+} ions, and this coordination interaction resulted in network formation to greatly improve on the modulus of the **P-Cur-Eu** system.

In order to confirm the contribution of hydrogen bonding, **P-Cur-CH₃** was synthesized to partially substitute N–H groups with N–CH₃ (Figure S7, Supporting Information). In specific,

both **P-Cur** and **P-Cur-CH₃** showed crossovers where $G' = G''$ at a frequency of ω_0 , but the modulus of **P-Cur** was much higher than that of **P-Cur-CH₃** (Figure 2a), indicating that the hydrogen bonding played an important role in improving mechanical property of **P-Cur** system. Furthermore, with addition of the Eu^{3+} , the crossover point was no longer observed in the coordinated systems. The G' further increased and became frequency independent, suggesting that the coordination induced crosslinked network was formed and the higher modulus of the material was primarily due to the formation of coordination crosslinks. We also introduced different molar ratios of $\text{Eu}(\text{CF}_3\text{SO}_3)_3$ into **P-Cur** and scaled the storage modulus to master curves (Figure S8, Supporting Information) by Williams–Landel–Ferry (WLF) equation. The shift factors were shown in Figure S9 in the Supporting Information. We noted that **P-Cur-Eu = 3:1** possessed a higher modulus, which was consistent with the theoretical ratio (3:1) between curcumin and Eu^{3+} judged from the above model compounds.

The mechanical properties of the films were measured at room temperature using tensile tests. All the coordinated materials showed typical rubber-like behaviors (Figure 2b). In specific, **P-Cur-Eu = 3:1** system possessed the highest tensile stress (1.8 MPa) and strain capability ($\approx 900\%$). All collected detailed data were summarized in Table S2 in the Supporting Information. The coordination was specific between Eu^{3+} and curcumin. Addition of other metals, such as Cu^{2+} and Tb^{3+} ,

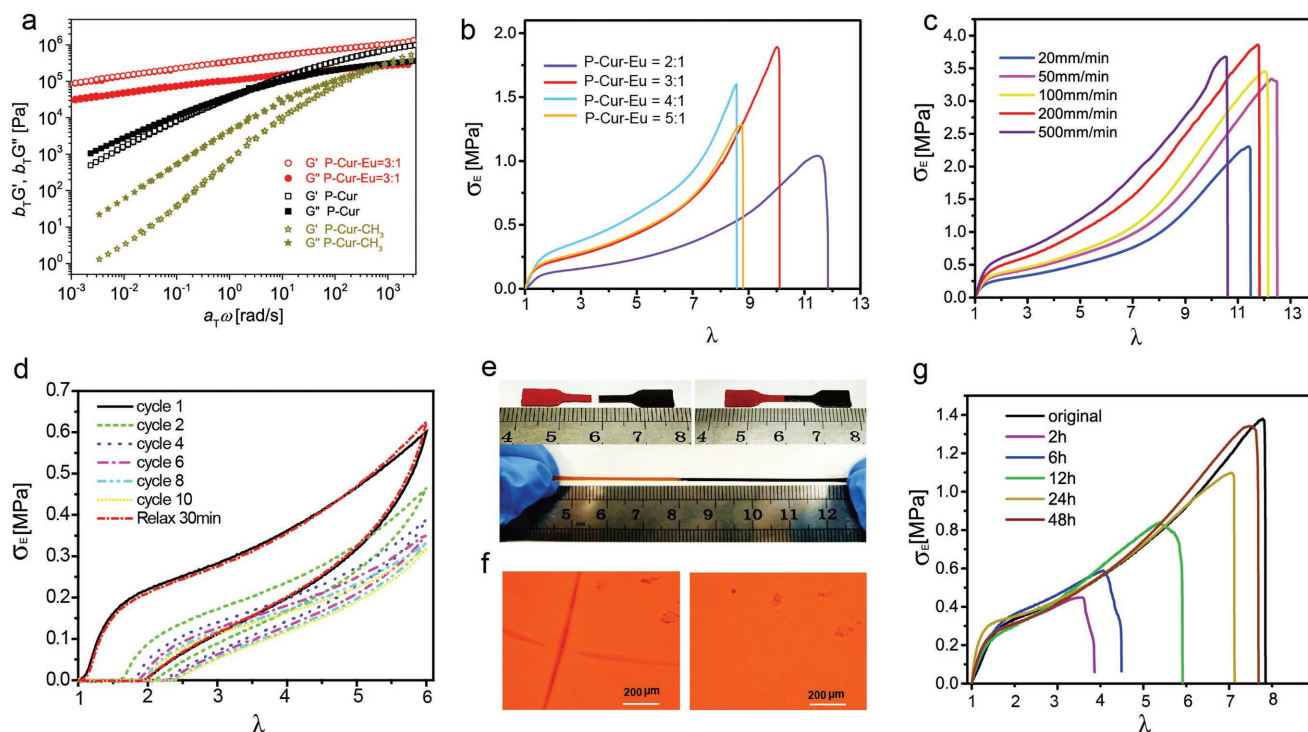


Figure 2. Mechanical and self-healing properties of **P-Cur-Eu**. a) Master curves of **P-Cur-Eu = 3:1**, **P-Cur**, and **P-Cur-CH₃** scaled by time–temperature superposition at a reference temperature 20 °C. b) Stress–strain curves of films prepared with different molar ratios of **P-Cur** ligand to **Eu (III)** with strain rate 20 mm min⁻¹. c) Engineering stress–strain curve of the film prepared with a **P-Cur** ligand to **Eu (III)** molar ratio of 3:1 (**P-Cur-Eu = 3:1**) stretched at different rates for a sample of width 5 mm, thickness 0.8 mm, and gauge length 5 mm. d) Recovery and cyclic loading of the film **P-Cur-Eu = 3:1**. The samples were loaded (500% strain), unloaded, and immediately reloaded ten times (tensile rate: 20 mm min⁻¹), and then the samples were allowed to rest for 30 min at 25 °C after releasing of the strain and stretched again (cycle 11). e) The cut pieces were aligned and joined together for healing at 25 °C for 24 h. Upon stretching the healed film manually, no cracking or breaking happened. f) Optical image of **P-Cur-Eu = 3:1** before and after healing at 25 °C for 24 h. Cut depth: 20–30% of its thickness 0.6 mm, scale bar: 200 μm. g) Films were cut into strips of about 5 mm in width, gauge length 3 mm, and height 1 mm. The samples were cut into completely separate pieces using a razor blade and they were aligned and healed at 25 °C for different healing times. Tensile tests were carried out with tensile rate of 20 mm min⁻¹.

did not show obvious improvement in strength (Figure S10, Supporting Information).

Next, we chose **P-Cur-Eu = 3:1** system for further investigations. We observed that the Young's modulus of the sample increased as the tensile rate increased (Figure 2c). Also, we observed that the materials showed good elastic performance and self-recovery property. Repeated cyclic tensile tests were performed as shown in Figure 2d, and it showed hysteresis and Mullins effect as derived from the volume fraction of soft segment increased during the initial cycle.^[25] We repeated stretching the sample to 6× its original length and unloading the sample by 10 cycles, and the energy density dissipated within the loop of the first cycle was estimated to be about 0.78 MJ m⁻³. With this value arbitrarily set as 100%, 67% of the energy dissipation was observed to be lost in cycle 2. This phenomenon had been also observed in other systems.^[26] The decrease of energy dissipation also appeared in subsequent cycles. These were attributed to the buildup of elastic deformation, which could not relax to equilibrium on the time scale of individual cycles. After 30 min relaxation, cycle 11 showed that ≈95% of the original energy dissipation observed in cycle 1 fully recovered (Figure S11, Supporting Information), indicating the sample regained its original mechanical performance. We speculated

that this observed excellent recovery in energy dissipative properties may be derived from the remaining **Eu–O** crosslinks, assisting in the reformation of hydrogen bonds. The fracture energy of the film was 2443 J m⁻² (Figure S12, Supporting Information), which was comparable to the tough elastomer reported by Creton and co-workers^[27] Furthermore, repeated stretching to various strains was also tested (Figure S13, Supporting Information). These observed mechanical behaviors indicated that the material possessed very good elastic performances.

P-Cur showed high autonomous healing efficiency (Figure S14, Supporting Information) but possessed low mechanical strength. Our polymer network was crosslinked with both dynamic metal coordination bonds and hydrogen bonding to confer autonomous self-healing ability. Specifically, **P-Cur-Eu = 3:1** exhibited spontaneous self-healing behavior at room temperature without external stimuli. In a typical self-healing experiment, for easy identification, one of the two pieces was stained with a black dye. After healing at room temperature for 24 h, the healed sample was observed to be able in sustaining a large strain once again (Figure 2e). In addition, any morphological changes around the damaged area were observed using an optical microscope. The notch on the film was barely distinguishable under the microscope (Figure 2f).

The self-healing process with different time was also shown in Figure S15 and Movie S1 in the Supporting Information. Next, we cut the films into two separate pieces and the two half films were gently brought back into contact with $\approx 40 \mu\text{m}$ of the residual scar on near-surface texture, and then the samples were healed at 25 °C (40% relative humidity (RH)) for different amounts of time. For all healing time, the stress–strain curves showed characteristic rubber-like behavior. Remarkably, the mechanically robust material could recover the yield stress and the toughness, even when it was cut into two pieces. In specific, its tensile strength was observed to be restored to 1.34 MPa (Figure 2g). The damaged sample was able to achieve 98% healing efficiency, as calculated by the strain at break and divided by that of the uncut samples after healing for 48 h at 25 °C (Figure S16, Supporting Information). We further investigated the influence of environmental factors on self-healing property. These experiments showed that the healing efficiency was improved as the contact area and temperature increased (Figures S17 and S18, Supporting Information). An increase in relative humidity did not decrease the strain capability of the healed samples but weakened the ultimate tensile strength after healing (Figure S19, Supporting Information). Figure S20 in the Supporting Information further illustrated the hypothesized self-healing mechanism for our robust elastomer. Our observed excellent stretching and self-healing properties were attributed to the introduced dynamic hybrid interactions, namely, M–L coordination and hydrogen bonding. Unlike the **P-Cur** system without M–L coordination, weak interactions would easily be disrupted at higher strain, resulting in chain sliding and hence weakening the modulus of the material.

Stretchable and self-healable conductors are critical in the field of stretchable electronics. Our group has previously reported the usage of nickel particles to achieve a self-healing conductor.^[28] Additionally, polymer/silver flake composites have shown high conductivity as elastic conductors.^[29]

Though a **P-Cur-Eu**/silver flake composite would have good compatibility with the substrate (**P-Cur-Eu**), it resulted in the poor self-healing efficiency (Figure S21, Supporting Information). Therefore, we chose **P-Cur**/silver flake composites to function a self-healable conductor instead. Procedures in preparing samples and the composition are described in the Experimental Section. Different amounts of the silver flakes were added to the polymer and the morphology of the composites was subsequently characterized by SEM (Figure 3a). For all our prepared test samples, silver flakes were dispersed in the polymer matrix homogeneously. We observed that conductive network could not form when the silver volume content was < 0.25 ; however, upon increasing the silver content to > 0.41 , the particles were sufficient to form a conductive network.

The conductivity of the composites is as expected from percolation theory (Figure 3b). Even when stretched, the high conductivity of the composites was maintained (Figure 3c). Resistances of both samples (at both 0.41 and 0.46 silver volume contents) increased less than $2\times$ of their original values at 200% strain. We also noted that at **0.46 silver**, the resistance increased to $4\times$ of the original resistance when the strain reached 400%.

Next, we characterized the mechanical and electrical self-healing properties of the conductive composites. First, the composites were cut into two distinct pieces. Next, the two

pieces were aligned and brought back together in close contact to allow heal at 25 °C. For example, **0.41 silver** was cut and allowed to reconnect. Both of the stress and elongation at break increased as the healing time increased, with the sample containing 0.41 silver failing at a strain of 200% after healing for 8 h at 25 °C (Figure S23, Supporting Information).

Remarkably, **0.41 silver** showed electrical self-healing properties in both the composites and the layer printed on the self-healing substrate **P-Cur-Eu = 3:1** (Figure S24, Supporting Information). After healing, we observed that a defect was left in the film and appeared upon initial loading. As the strain increased, the defect propagated gradually since the applied stress was primarily concentrated around the defect area. We observed that our prepared composite material failed when the strain exceeded 90% (Figure 3d). It was noted that the self-healing conductor could reach a high conductivity (46 S cm^{-1}) and possessed 90% fracture strain after healing, which is competitive when compared with the reported self-healable conductors (Figure S25, Supporting Information).

Using our prepared composite material, we proceeded to fabricate a self-healing conductor, as shown in Figure 3e. A 1.5 V voltage was applied on a **P-Cur/Silver** (0.41 volume) composite sheet and connected with a light-emitting diode (LED). As expected, the LED turned off when the film was cut. However, after healing the conductor for 24 h at 25 °C, the light was observed to turn back on again.

With our elastic and self-healable conductor, we proceeded to demonstrate a stretchable and self-healable touch pad. Our demo stretchable touch pad was comprised of a 3×3 capacitive sensor array (Figure 4a), using **P-Cur-Eu = 3:1** as the self-healing dielectric substrate. The capacitive sensor array shared a set of common bottom electrodes, and blade-coating method was used to pattern the self-healable silver paste for the top electrodes. With the fabricated touch pad, we observed that when the human finger touches each pixel, the capacitance between the top and bottom electrode changes (Figure 4c). The capacitance change could also be read at different strain levels (Figure S26, Supporting Information). We reasoned that it was due to the electrostatic interference of human finger to surrounding environment (simulation in Supporting Information and Figures S27 and S28, Supporting Information). Such changes could then be read by a specifically designed signal conditioning circuit (SCC). In the SCC, a 2 MHz oscillator was generated to function as the source to read the impedance of our capacitance touch pad sensor array. The signal then traveled through an envelope detector (a combination of D01, C02, and R0) to exhibit its amplitude. After digitization using a 1 bit analog–digital converter (ADC), such signal was processed by a microcontroller. The microcontroller recognized the pixel as to where the signal originated, and it would then compare the received code with the originally stored or programmed security code. Depending on the input five-sequence passcode, the microcontroller would either generate a green LED if the two codes were matched up or generate a red LED for mismatched codes (Figure 4d; Supplementary Movie 2). We also noted that all the needed read out circuit was neatly integrated into a single printed circuit board.

Next, to investigate its healing ability, we first tested the self-healing property of a single pixel capacitor. As shown in Figure 4e, the capacitance changed by finger touch could

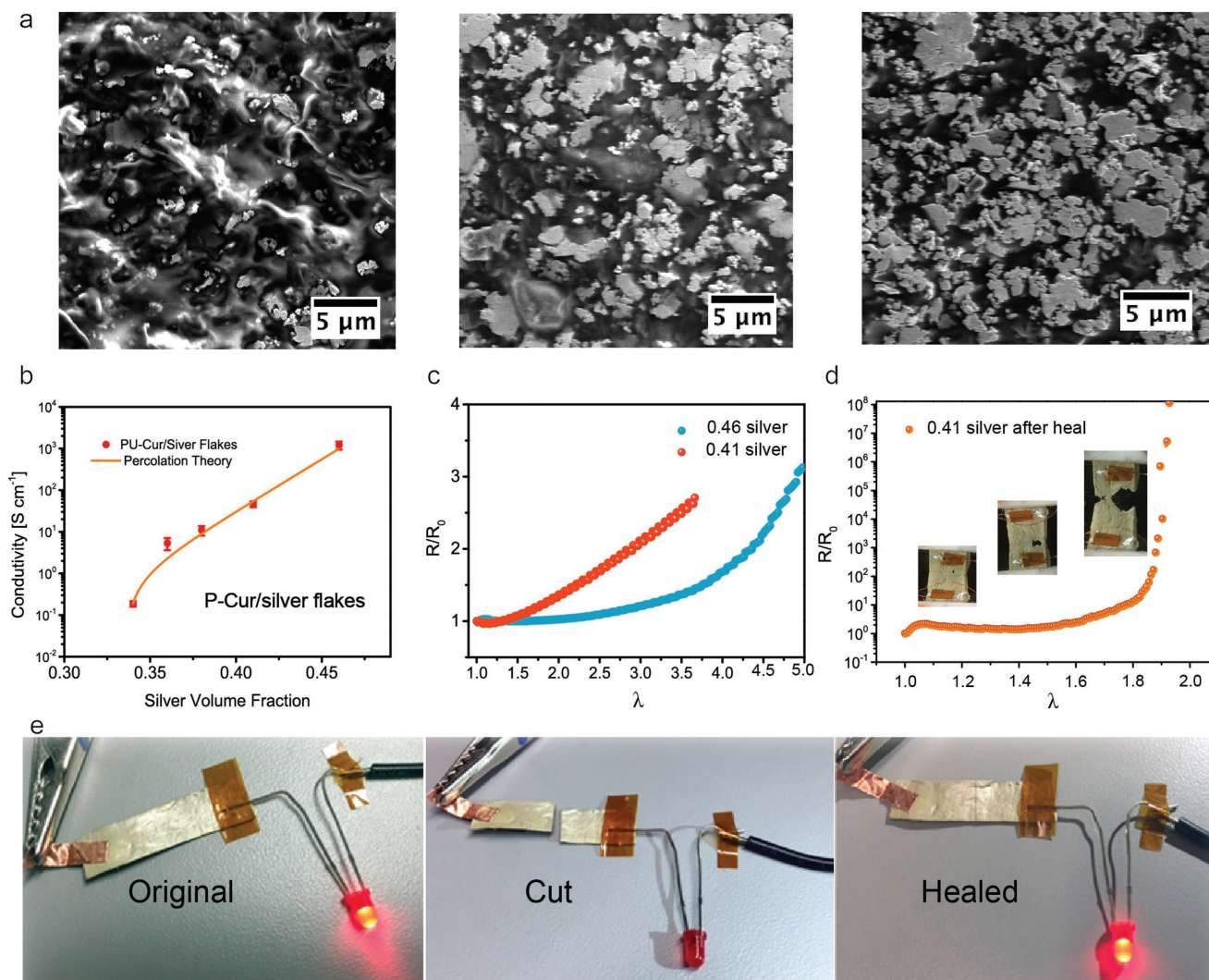


Figure 3. Self-healing conductive composites. a) Cross-sectional SEM images of **P-Cur/Silver** composites. The volume fractions of the silver flakes are 0.25, 0.41, and 0.46 separately. b) Electrical conductivity as a function of silver flake content from four-point probe measurements. Error bars represent standard deviation from five samples. c) Resistance of the **P-Cur/silver flake** composites upon stretching. d) Resistance of the self-healed **P-Cur/silver** composites during stretching. e) Demonstration of the healing process for a conductive composite with an LED in series with a self-healing electrical conductor.

recover to its original level after scratching and healing for ≈ 40 s. Furthermore, we used a razor blade to sever the device into two parts. We then reattached the two distinct pieces together and allowed healing at room temperature for 24 h (Figure 4f). Interestingly, we observed that high conductivity was highly preserved after healing (Figure S29, Supporting Information). We next input the correct passcode to the pad to ensure its functionality. Furthermore, even when the healed device was stretched to 80% strain, the device remained functional (Figure 4g and Supplementary Movies 3 and 4).

In summary, we demonstrate that by using both Eu-curcumin coordination and H-bonding, we are able to achieve a material that possesses self-healing property with good elastic properties, such as high stress at break, high stretchability, and good recoverability. We ascribe this performance

improvement to the dual-dynamic chemical interaction system, which is able to generate interchain crosslinking and microphase-separated structures. Even in the absence of light or heat stimuli, the damaged film can achieve very high healing efficiency after 48 h at 25 °C, along with a restoration up to 98% in its tensile strain. After incorporating conductive silver flakes into our self-healable polymer, the resulting composite materials show both excellent mechanical and electrical self-healing properties. These materials ultimately allowed for the construction of a stretchable and self-healable capacitive touch pad.

Supporting Information

Supporting Information is available from the Wiley Online Library or from the author.

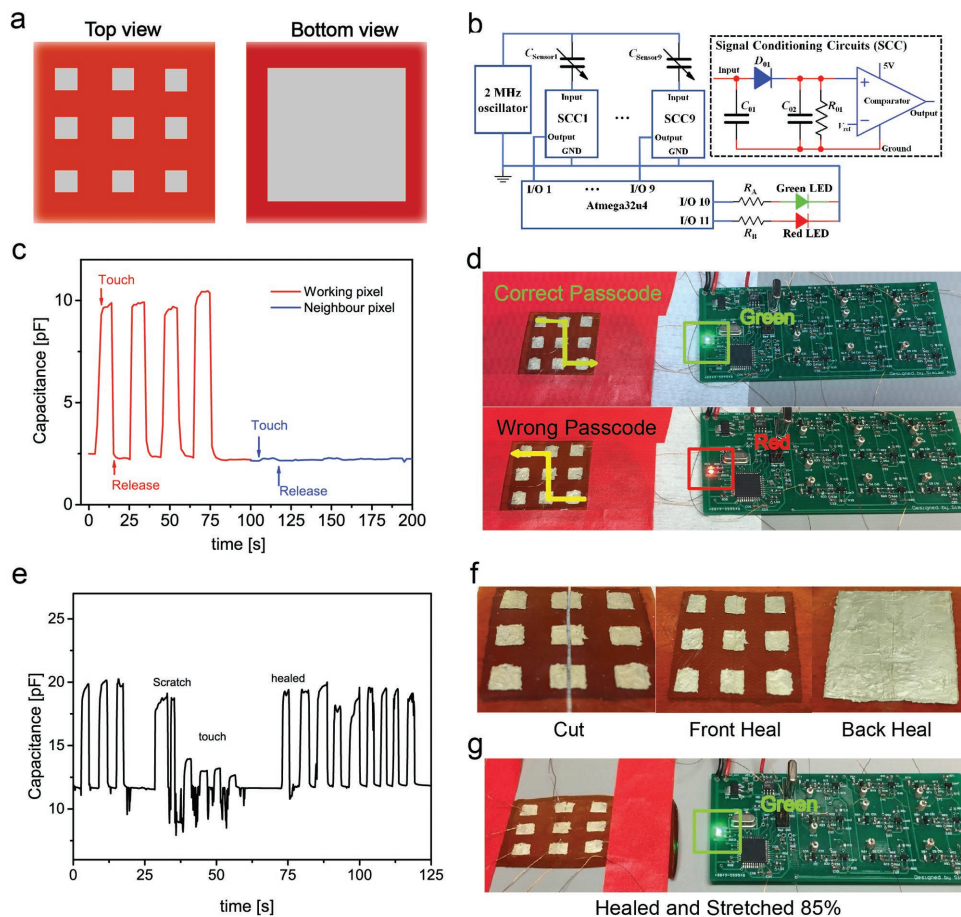


Figure 4. Application in a capacitive touch pad device. a) Diagram of the self-healing device, which was composed of three layers: the top layer with nine square pixels in the size of $5\text{ mm} \times 5\text{ mm} \times 0.02\text{ mm}$ was made of the self-healing conductor of **0.41 silver**. The intermediated layer was made of **P-Cur-Eu = 3:1** with a thickness of 0.5 mm . The bottom layer in the size of $3\text{ cm} \times 3\text{ cm} \times 0.02\text{ mm}$ was made of the same self-healing conductor as the top layer. b) Circuit diagram of the designed self-healing touch pad. c) Capacitance change when finger touches on a single working pixel and one neighbor pixel. d) Photos illustrating as how the device functions. The upper picture showed the green light in PCB board turned on after a correct passcode is pressed. The bottom figure showed the red light turned on after a wrong passcode is input. e) Capacitance before and after scratching and healing. f) Cutting the device by a razor blade along the middle of the three pixels and then realigning the two cut pieces back together and healing at room temperature for 24 h. The front and back image after heal was shown. g) After stretching the healing device 85% strain along the vertical direction to the cutting line, the green light can then be turned on after the correct passcodes were input.

Acknowledgements

Q.Z., S.N., and L.W. contributed equally to this work. Q.Z., S.N., L.W., X.J., and Z.B. conceived the concept and the experiments. Q.Z., S.N., and L.W. develop the fabrication processes. Q.Z., S.N., L.W., J.L., S.C., Y. C., R. D., and Y.L. performed the experiments and analyzed the data. Z.B. and X.J. supervised the project. Q.Z., S.N., L.W., J.B.-H.T., X.J., and Z.B. wrote the manuscript. All authors reviewed and commented on the manuscript. S.N. and Z.B. acknowledge support from Samsung Electronics. Q.Z. thanks the National Natural Science Foundation of China (Grants 21404056), and China Scholarship Council (201606195042) funded the expense and the project in visiting Stanford University. Part of the work was supported by the Fundamental Research Funds for the Central Universities. Part of this work was performed at the Stanford Nano Shared Facilities (SNSF), supported by the National Science Foundation under award ECCS-1542152.

Conflict of Interest

The authors declare no conflict of interest.

Keywords

capacitive sensors, dual interaction, elastomers, self-healing

Received: March 3, 2018

Revised: June 6, 2018

Published online:

- [1] a) T. Someya, Z. Bao, G. G. Malliaras, *Nature* **2016**, *540*, 379; b) S. J. Benight, C. Wang, J. B. H. Tok, Z. A. Bao, *Prog. Polym. Sci.* **2013**, *38*, 1961.
- [2] Z. Bao, *Mater. Res. Soc. Bull.* **2016**, *41*, 897.
- [3] M. Kaltenbrunner, T. Sekitani, J. Reeder, T. Yokota, K. Kuribara, T. Tokuhara, M. Drack, R. Schwodiauer, I. Graz, S. Bauer-Gogonea, S. Bauer, T. Someya, *Nature* **2013**, *499*, 458.
- [4] D.-H. Kim, J.-H. Ahn, W. M. Choi, H.-S. Kim, T.-H. Kim, J. Song, Y. Y. Huang, Z. Liu, C. Lu, J. A. Rogers, *Science* **2008**, *320*, 507.
- [5] a) B. Ghosh, M. W. Urban, *Science* **2009**, *323*, 1458; b) A. Rekondo, R. Martin, A. Ruiz de Luzuriaga, G. Cabañero, H. J. Grande,

- I. Odriozola, *Mater. Horiz.* **2014**, *1*, 237; c) J. A. Neal, D. Mozhdzhi, Z. Guan, *J. Am. Chem. Soc.* **2015**, *137*, 4846; d) H. Ying, Y. Zhang, J. Cheng, *Nat. Commun.* **2014**, *5*, 3218; e) S. Ji, W. Cao, Y. Yu, H. Xu, *Angew. Chem., Int. Ed.* **2014**, *53*, 6781.
- [6] a) A. M. Kushner, J. D. Vossler, G. A. Williams, Z. Guan, *J. Am. Chem. Soc.* **2009**, *131*, 8766; b) A. Feula, A. Pethybridge, I. Giannakopoulos, X. Tang, A. Chippindale, C. R. Siviour, C. P. Buckley, I. W. Hamley, W. Hayes, *Macromolecules* **2015**, *48*, 6132; c) P. Cordier, F. Tournilhac, C. Soulie-Ziakovic, L. Leibler, *Nature* **2008**, *451*, 977; d) J. Liu, C. S. Tan, Z. Yu, Y. Lan, C. Abell, O. A. Scherman, *Adv. Mater.* **2017**, *29*, 1604951; e) Y. Lin, G. Li, *J. Mater. Chem. B* **2014**, *2*, 6878; f) M. Burnworth, L. Tang, J. R. Kumpfer, A. J. Duncan, F. L. Beyer, G. L. Fiore, S. J. Rowan, C. Weder, *Nature* **2011**, *472*, 334; g) T. L. Sun, T. Kurokawa, S. Kuroda, A. Bin Ihsan, T. Akasaki, K. Sato, M. A. Haque, T. Nakajima, J. P. Gong, *Nat. Mater.* **2013**, *12*, 932.
- [7] a) S. Wu, J. Li, G. Zhang, Y. Yao, G. Li, R. Sun, C. Wong, *ACS Appl. Mater. Interfaces* **2017**, *9*, 3040; b) M. V. Biyani, E. J. Foster, C. Weder, *ACS Macro. Lett.* **2013**, *2*, 236.
- [8] a) Y.-L. Liu, T.-W. Chuo, *Polym. Chem.* **2013**, *4*, 2194; b) Z. Xu, Y. Zhao, X. Wang, T. Lin, *Chem. Commun.* **2013**, *49*, 6755.
- [9] G. Hong, H. Zhang, Y. Lin, Y. Chen, Y. Xu, W. Weng, H. Xia, *Macromolecules* **2013**, *46*, 8649.
- [10] Y. Yanagisawa, Y. Nan, K. Okuro, T. Aida, *Science* **2018**, *359*, 72.
- [11] A. L. Larsen, K. Hansen, P. Sommer-Larsen, O. Hassager, A. Bach, S. Ndoni, M. Jorgensen, *Macromolecules* **2003**, *36*, 10063.
- [12] D. E. Hanson, J. L. Barber, *Contemp. Phys.* **2015**, *56*, 319.
- [13] L. J. Prins, D. N. Reinhoudt, P. Timmerman, *Angew. Chem., Int. Ed.* **2001**, *40*, 2382.
- [14] Z.-Y. Zeng, Y.-S. Wang, S. D. Chao, *Comput. Theor. Chem.* **2017**, *1113*, 1.
- [15] E. Yildirim, M. Yurtsever, *Comput. Theor. Chem.* **2014**, *1035*, 28.
- [16] J. R. Wu, L. H. Cai, D. A. Weitz, *Adv. Mater.* **2017**, *29*, 1702616.
- [17] S.-M. Kim, H. Jeon, S.-H. Shin, S.-A. Park, J. Jegal, S. Y. Hwang, D. X. Oh, J. Park, *Adv. Mater.* **2018**, *30*, 1605325.
- [18] T. Wang, Y. Zhang, Q. Liu, W. Cheng, X. Wang, L. Pan, B. Xu, H. Xu, *Adv. Funct. Mater.* **2018**, *28*, 1705551.
- [19] X. Liu, G. Su, Q. Guo, C. Lu, T. Zhou, C. Zhou, X. Zhang, *Adv. Funct. Mater.* **2018**, *28*, 1706658.
- [20] Y. L. Chen, A. M. Kushner, G. A. Williams, Z. B. Guan, *Nat. Chem.* **2012**, *4*, 467.
- [21] a) D. Mozhdzhi, S. Ayala, O. R. Cromwell, Z. Guan, *J. Am. Chem. Soc.* **2014**, *136*, 16128; b) C.-H. Li, C. Wang, C. Keplinger, J.-L. Zuo, L. Jin, Y. Sun, P. Zheng, Y. Cao, F. Lissel, C. Linder, X.-Z. You, Z. Bao, *Nat. Chem.* **2016**, *8*, 619; c) S. C. Grindy, R. Learsch, D. Mozhdzhi, J. Cheng, D. G. Barrett, Z. Guan, P. B. Messersmith, N. Holten-Andersen, *Nat. Mater.* **2015**, *14*, 1210.
- [22] S. Velankar, S. L. Cooper, *Macromolecules* **1998**, *31*, 9181.
- [23] J. Mattia, P. Painter, *Macromolecules* **2007**, *40*, 1546.
- [24] Y. Mawani, C. Orvig, *J. Inorg. Biochem.* **2014**, *132*, 52.
- [25] J. A. C. Harwood, A. R. Payne, *J. Appl. Polym. Sci.* **1968**, *12*, 889.
- [26] H. Zhang, Y. Chen, Y. Lin, X. Fang, Y. Xu, Y. Ruan, W. Weng, *Macromolecules* **2014**, *47*, 6783.
- [27] E. Ducrot, Y. Chen, M. Bulters, R. P. Sijbesma, C. Creton, *Science* **2014**, *344*, 186.
- [28] B. C. K. Tee, C. Wang, R. Allen, Z. Bao, *Nat. Nanotechnol.* **2012**, *7*, 825.
- [29] N. Matsuhisa, D. Inoue, P. Zalar, H. Jin, Y. Matsuba, A. Itoh, T. Yokota, D. Hashizume, T. Someya, *Nat. Mater.* **2017**, *16*, 834.